Conceptual Model of the Puna Geothermal System

Drew Spake, Zach Reynolds, Derek Caro, Nick Prina, John Murphy, Adam Johnson, Paul Spielman, Robin Zuza, Simon Webbison

Ormat Technologies, Inc.

Keywords

Geology, Drilling, Conceptual Model, Image Log Analysis

ABSTRACT

The Puna Geothermal Venture (PGV) is a 38-MW combined cycle power plant producing from a two phase, liquid-dominated, 280-320°C (±535-610°F) resource located at a prominent left-step in Kilauea's East Rift Zone on the Island of Hawai'i. Drilling results and interpretation of available geoscientific datasets reveal a deep reservoir with fracture-dominated permeability controlled primarily by rift-parallel fractures with some contribution from rift-cutting features.

The 2018 Kilauea eruption forced plant shutdown and resulted in a recovery campaign which brought the plant back online in 2020. Following plant restart a new drilling campaign was completed, adding two new wells to the production field and one new well to the injection field and bringing PGV generation to over 32 MW for the first time since the eruption. An acoustic borehole image log was successfully acquired for the first time at PGV during this drilling campaign, providing new insights into subsurface conditions and permeability controls. In this paper we integrate available geologic, geophysical, and geochemical to provide a conceptual framework for the PGV system.

1. Introduction

Exploration for naturally occurring geothermal systems as a source of independent power production has been ongoing in the state of Hawai'i since at least the early 1960s. Numerous state and federally funded projects have studied Hawai'i's geothermal potential through a variety of geological, geophysical, and geochemical surveys, as well as exploration drilling to test hypotheses resulting from surface exploration (e.g., Furumoto et al., 1977; Thomas, 1986; Lautze et al., 2017; Warren et al., 2023). The Island of Hawai'i was the focus of early exploration efforts due to its active volcanism and the presence of surface manifestations of geothermal systems, such as hot springs, which other islands lack. Kilauea volcano and its associated rift zones are the most favorable regions for Hawaiian geothermal exploration due to the colocation of necessary elements for the formation of hydrothermal systems: elevated shallow heat flow (from young volcanism), a

fluid-saturated subsurface (implied by the high annual rainfall and location on an oceanic island), and permeable fluid pathways to support natural convective processes (suggested by active tectonic dilation along the rift zones).

Geothermal exploration on the Island of Hawai'i began in 1961 with the drilling of four exploration wells by Hawaii Thermal Power Company in Kilauea's Lower East Rift Zone (LERZ) near a prominent left step in the rift zone's fissures. The wells (TH-1, -2, -3, & -4) encountered elevated groundwater temperatures ranging from 109° to 203°F (43° to 95°C) at depths from 216 to 686 ft but were plugged and abandoned, lacking temperatures high enough for energy production (DPED, 1982). Following an extensive geophysical survey of the LERZ from 1973-1975, the Hawai'i Geothermal Project utilized federal, state, and county grant funds to drill the HGP-A resource discovery well near Pu'u Honua'ula, the initial eruptive fissure for the 1955 LERZ eruption. HGP-A was completed in April 1976 to 6450 ft (1966 m) measured depth (MD) with a bottom hole temperature of 676°F (358°C) (Takahashi et al., 1985). The well produced 110 kph at 166 psig with ~43% steam fraction to a 3MW turbine generator from 1981-1989, marking the onset of geothermal energy production in Hawai'i. Additional exploration drilling along the LERZ during the 1980-1990s by competitor companies and the State of Hawai'i/University of Hawai'i demonstrated the existence of high temperatures along the LERZ, but high permeabilities were never encountered and production was not sustained from any of the Lanipuna, Ashida, or Scientific Observation Hole (SOH) locations (Figure 1).

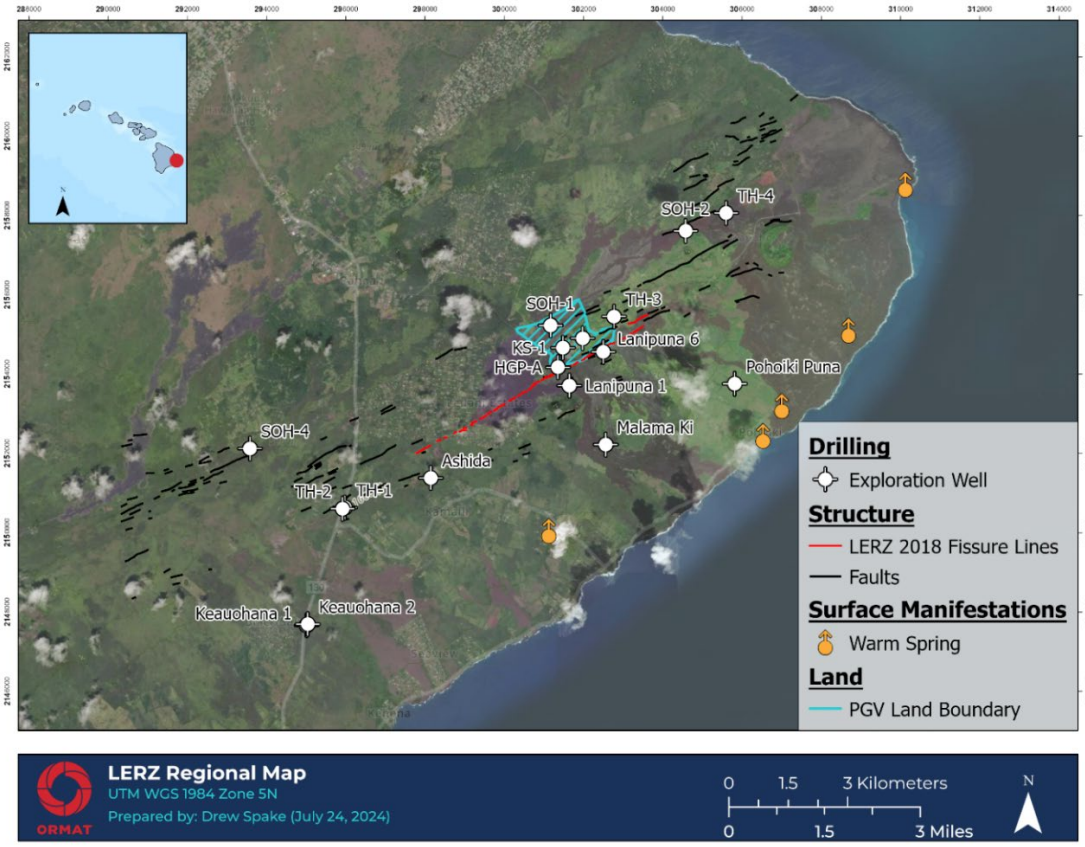

Figure 1: Regional map of Kilauea's Lower East Rift Zone. The PGV lease area is shown in hatched blue, with faults shown in black (Moore and Trusdell, 1991) and fissures from the 2018 eruption in red (Zoeller et al., 2020). Geothermal exploration wells are shown in white, and warm springs in orange.

PGV was the first and only commercially productive geothermal power plant in Hawaii and provided 31% of the island's electrical demand in 2017. PGV began commercial operation of a >600°F (315°C) naturally occurring geothermal system with an Ormat-supplied 30 MW combined cycle power plant with 100% reinjection of produced fluids in 1993. The project was acquired by Ormat in June 2004, and over the years generation has increased by upgrading the facility, through resource development, and with the addition of two bottoming OECs (Ormat Energy Converter) which produced more energy from the brine. As of 2012, the facility was comprised of a combined cycle (steam turbine with binary condenser) air cooled plant and two brine binary units with a nameplate capacity of 38 MW. The plant operated continuously from startup in 1993 until plant shutdown in May 2018 due to a volcanic eruption along the LERZ. Recovery efforts to the facility began in early 2019 following cessation of the eruption in late September 2018. The plant was brought back online in November 2020 after an extensive campaign to restore both the power plant and wellfield, which included workovers, re-drills, and initially the drilling of 3 new wells.

Following plant restart, a drilling campaign from 2022-2023 successfully three new wells, with the additional production brine helping to increase PGV's generation to >32 MW for the first time since the eruption. As part of the planned completion testing for the campaign an acoustic borehole image log was acquired in the northernmost well, the first successful image log at PGV.

As of this writing (June 2024), there have been 20 full-sized "KS" (Kapoho State) wells drilled at PGV with a total of 39 discrete legs considering original holes (OH), twins (e.g., KS-1A), multi-leg completions (ML), redrills (RD), and sidetracks (ST). Production wells are primarily clustered on the southern side of the wellfield, with injection wells primarily on the northern side of the field (Figure 2).

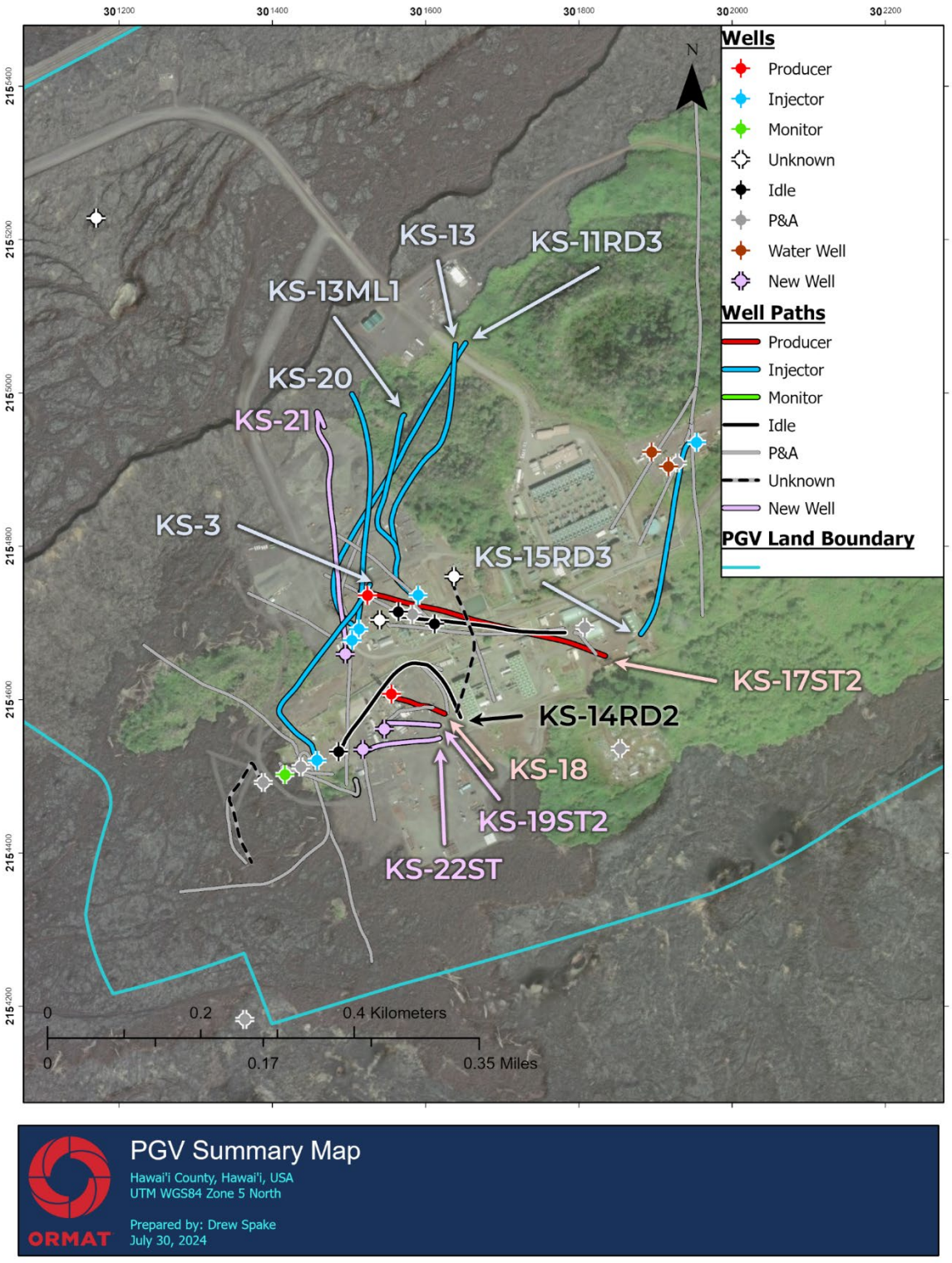

Figure 2: PGV wellfield map. Directional well paths are shown with colors corresponding to the well's status, with new wells completed during the 2022-2023 drilling campaign indicated separately. The bottom hole location of new wells and active production/injection wells are labeled (other wells left unlabeled for clarity).

2. Geology

2.1 Regional Geology and Tectonic Setting

The hydrothermal system at PGV is located in a volcanic rift zone associated with the Kilauea volcano on the Island of Hawai'i. The Hawaiian-Emperor island chain is a string of 8 major and 129 minor islands and seamounts formed by a mantle plume hot spot over the past ±70 MA (Wilson, 1963). The Island of Hawai'i is the youngest, southernmost member of the archipelago and encompasses five major shield volcanoes (from oldest to youngest: Kohala, Mauna Kea, Hualālai, Mauna Loa, & Kilauea). An older, sixth volcano, Māhukona, lies beneath sea level off the northwestern tip of the island, while Kama'ehuakanaloa (formerly Lō'ihi), represents active growth of the newest volcano in the chain southeast of Kilauea (Sherrod et al., 2021).

Magma supply to Hawaiian volcanoes originates with upwelling of mantle melt at an intraplate "hot spot" (Wilson, 1963; Morgan, 1971). On the Island of Hawai'i, Kilauea and Moana Loa share magma supply from the hot spot but likely have separate, though proximal, storage chambers (Poland et al., 2014). The general model for Kilauea's magma plumbing system is that magma generated in the mantle at 30-60 km depth ascends and is stored at neutral buoyancy in reservoirs that are 2-4 km beneath the summit and almost wholly molten rift zones at 3-10 km beneath the surface (Eaton and Murata, 1960; Ryan, 1988) (Figure 3).

Hawaiian volcanoes are built through successive stages of volcanism, quiescence, and erosion. An idealized model of Hawaiian volcano evolution involves four eruptive stages: (1) a pre-shield submarine alkalic stage, (2) a tholeiitic shield-building stage, depositing ≥95% of the volume of the volcano, (3) a post-shield alkalic stage which deposits a thin cap of alkalic basalt and differentiated lavas, and (4) an alkalic rejuvenation stage characterized by isolated vent eruptions following several million years of dormancy and erosion (Clague and Dalrymple, 1987). Deposits found on the Island of Hawai'i represent stages 1-3, with the active Mauna Loa and Kilauea depositing primarily tholeiitic basalts through shield-stage volcanism (Sherrod et al., 2021).

Kilauea's oldest deposits are ±275 ka alkalic, pre-shield submarine basalts which were sampled from the southern slope of the volcano by remotely operated submersibles, presumably representing submarine lava flows (Lipman et al., 2002). The SOH-1 exploration core hole drilled on the eastern flank of the volcano records a transition from subaerial to submarine deposits at ±551 m below sea level in a sequence comprised entirely of tholeiitic lava flows and dikes (Trusdell et al., 1999; Sherrod et al., 2021). Surface mapping shows that Kilauea's subaerial stratigraphy is composed of three major units (oldest-youngest): (1) the Hilina Basalt, (2) the Pahala Ash, and (3) the Puna Basalt (Sherrod et al., 2021). The Hilina Basalt is exposed only in fault scarps located along the southern flank of the volcano, while the Puna Basalt covers nearly the entire surface of Kilauea (Langenheim and Clague, 1987; Sherrod et al., 2021).

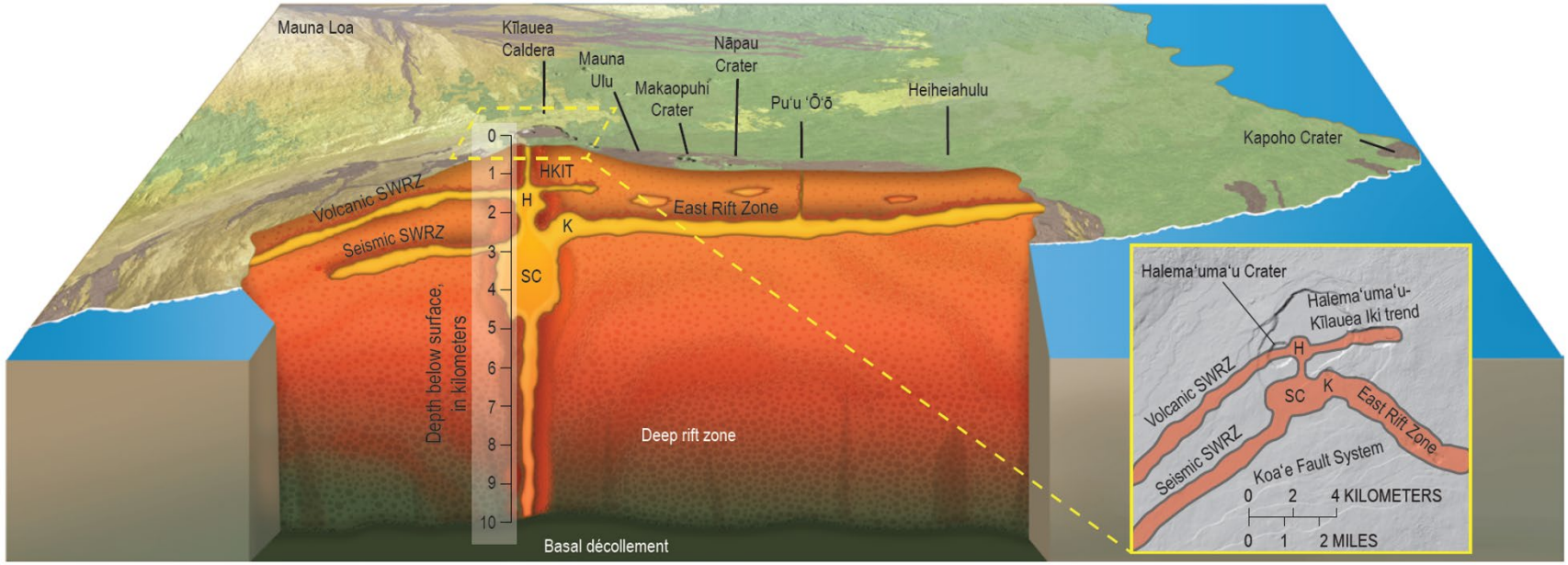

Figure 3: Illustration of Kilauea's magma plumbing system. Schematic cross section depicts the magma pathways and storage areas (exaggerated in size). K, Keanakāko'i reservoir; SC, south caldera reservoir; SWRZ, Southwest Rift Zone. Schematic viewing direction is from south to north. Plan view gives the relations of magma pathways to surface features and topography in the vicinity of Kilauea Caldera. (Figure and text reproduced from Poland et al., 2014).

Kilauea is cut by two rift zones which emanate from the summit caldera: the East Rift Zone (ERZ) and Southwest Rift Zone (SWRZ) (Figure 4). The two rift zones are bridged by the Koa'e Fault and Hilina Fault zones, deeply rooted normal fault systems accommodating southeastward displacement along the rift zones (Lipman et al., 1985, Duffield, 1975). Beginning in the 1950s, the ERZ became the most active part of Kilauea's magmatic system (Poland et al., 2014). Magma movement along the rift is facilitated by seaward extension of Kilauea's mobile southern flank, which acts to dilate the rift zone (Patrick et al., 2020). Motion of the south flank is likely accommodated by slip along a basal decollement 6-11 km deep at the interface between pre-Mauna Loa oceanic crust and the overlying volcanic edifice (Lipman et al., 1985).

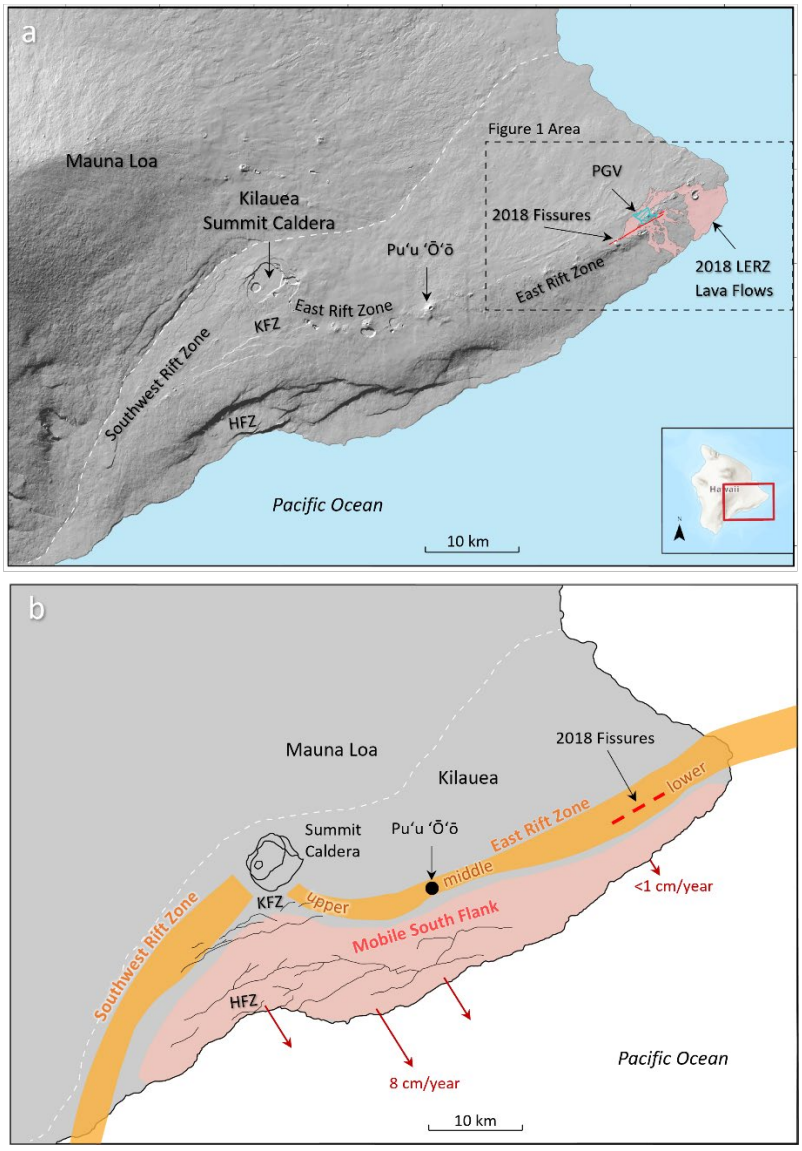

Figure 4: (a) Map of Kilauea volcano. The approximate boundary between Mauna Loa and Kilauea lavas is denoted by the dashed white line and the area of Figure 1 is shown by the black dashed box with PGV's location indicated in hatched blue. (b) Schematic structural map of Kilauea volcano showing the summit region and two rift zones. The mobile south flank exhibits steady southeast motion and is tightly coupled with the rift magmatic system. KFZ: Koa'e Fault Zone. HFZ: Hilina Fault Zone. (Figure modified from Patrick et al., 2020).

The East Rift Zone extends southeast from the summit caldera for approximately 7 km, then trends ±063° (N63°E) toward and beyond the end of the land surface. The rift is loosely subdivided into upper, middle, and lower sections and is one of the main conduits for lateral migration of magma from the holding chamber beneath Kilauea's summit caldera, with eruptions in the lower portion of the rift having occurred as recently as 1790, 1840, 1955, 1960, 1961, and 2018 (Moore and Trusdell, 1991).

The subaerial portion of the LERZ strikes 063°, is 3-4 km wide and about 23 km long, extending for an additional 70 km offshore as the submarine Puna Ridge. The LERZ is a constructional ridge characterized by low spatter deposits and cones up to ~200 ft (60 m) high (Moore and Trusdell, 1991). Its elevation gently decreases from southwest to northeast and ranges from a high of 1,713 ft (522 m) above sea level at Heiheiahulu to sea level at Cape Kumukahi (Swanson et al., 1976). The overall vent and fracture lineaments align strongly along the 063° trend and typically exhibit a pattern of en echelon step-overs.

Underlying the surface expression of the ERZ is a much broader (±12- 20 km wide) intrusive dike complex inferred by gravity (Broyles et al., 1979) and magnetic data (Kinoshita et al., 1963). This complex is thought to consist of an aggregate of closely spaced, parallel to subparallel, vertical to steeply dipping dikes intruded into a sequence of Mauna Loa and Kilauea lava flows. Individual dikes are likely <1 m to 5 m in width, though may be vertically and laterally extensive (Swanson et al., 1976; Wilson and Head, 1988).

2.2 Local Geology and Structure

All the rocks in the vicinity of PGV are Holocene tholeiitic basalts with varying abundances of olivine and pyroxene phenocrysts reflecting the relative amount of fractionation of magmas in subsidiary magma chambers along the rift zone (Moore and Trusdell, 1991; Langenheim and Clague, 1987). Pahoehoe and a'a lava flows as well as spatter deposits and small cinder cones dominate the landscape, representing eruptive events from about the year 1601 up to the most recent eruption in 2018, which overran part of the PGV wellfield and covered older deposits. Two small cinder cones and associated spatter deposits known as Pu'u Honua'ula from an eruption ±373 years before present form prominent hills on the PGV property. The power plant is constructed on a small topographic high formed by flows from the 1955 eruption which emanated from fissures at the base of the two cones. This small plateau prevented the plant from being consumed by the 2018 lava flows.

Eruptive vents on the southern side of the LERZ are commonly en echelon and right-stepping in the region west of Puulena Crater (~800 m southwest of the PGV lease). The linear alignment of vents abruptly terminates here, shifting left (northwest) by ~1 km, where they resume the 063° trend but are organized in left-stepping en echelon arrangement. The left step is well documented by seismic and magnetic datasets, however no transverse faults striking perpendicular to the main rift trend have been identified. The differential motion of the southern flank may result in failure of structural blocks bound by NW-striking faults, causing the stepover (Moore, 1992).

2.3 Downhole Geology and Structure

Subsurface geology is informed by the relatively high-density drilling over the small areal extent at the PGV project area, with additional context and regional constraints provided by publications on the early exploration wells, particularly HGP-A and the SOH holes.

Wells drilled at PGV document 3 major correlatable units, in order from shallowest to deepest: l) subaerial basalt flows 2) a transitional, near-shore assemblage dominated by hyaloclastites, and 3) submarine pillow basalts. Diabase dikes are found throughout the stratigraphic sequence but increase in frequency and width with depth. These lithologic assemblages are not internally homogeneous, and geologists working at Puna have divided the basalt stratigraphy into the following primary divisions based on physical characteristics: scoria (cinders), lavas (vesicular, aphanitic), hyaloclastite, diabase dikes (porphyritic), highly altered (observable parent texture i.e., vesicular or aphanitic) and clay (indistinguishable parent texture commonly associated with hyaloclastite and/or tephra). The hydrothermal reservoir is hosted within fractured submarine basalt flows and diabase dikes starting about 4200 ft (1280 m) below ground level (bgl) (approximately -3600ft/-1100 rSL (relative to sea level)).

The depositional environment directly affects the physical appearance of all three basalt types. Subaerial basalts, mostly a'a and pahoehoe, occur as solid flows separated by rubblized interflow breccias or sometimes totally fragmented and rubblized flows. Submarine basalt flows occur as dense conglomerates of pillows and pillow fragments infilled by ocean floor clays and silica. Dikes are typically coarser grained tabular bodies that intruded pre-existing flow basalts. Hyaloclastites are deposits of grit to sand sized granular glass fragments formed when hot, fluid basalt flows into the ocean creating phreatic explosions. The hyaloclastite material may be deposited off or near shore as black sand beaches or on shore as littoral cones and tuff rings depending on the prevailing winds and intensity of the lava-water reaction. Primary olivine tholeiites as well as differentiated basalts can be found as subaerial, submarine, hyaloclastite, or intrusive dike deposits.

Permeable fractures are commonly, but not ubiquitously, associated with the intersection of diabase dikes. Dike rock is recognized by its relatively coarse grained, hypidiomorpic, subhedral texture, its fresh, unaltered appearance, and general scarcity of secondary mineralization. In many wells the permeable fractures were encountered in the footwall side of a diabase dike after drilling through several tens of feet of diabase.

Dikes and permeable fractures are primarily interpreted to be aligned with the local strike of the LERZ (063°) and subvertical or steeply northwest dipping. Permeable fractures at PGV are generally named for the first well to have intersected the feature, e.g., the KS-5 Fracture hosts current production from the KS-19ST2 and KS-22ST wells. Key production fractures include the KS-5, KS-8, and KS-14 Fractures, and injection is hosted in the 1955 Fissure (distinguished by discrete North and South fracture zones), KS-3, and KS-20 Fractures.

In addition to the SW-NE striking features, the conceptual and numerical models include permeable pathways oriented perpendicular to the rift (NW-SE) (Murphy et al., 2024), which is supported by observed tracer return pathways and consistent with PGV's location at the major left-step in the LERZ (Figure 5). A key purpose for image log acquisition during the 2022-2023 drilling campaign was to establish if such fractures are identifiable in the subsurface.

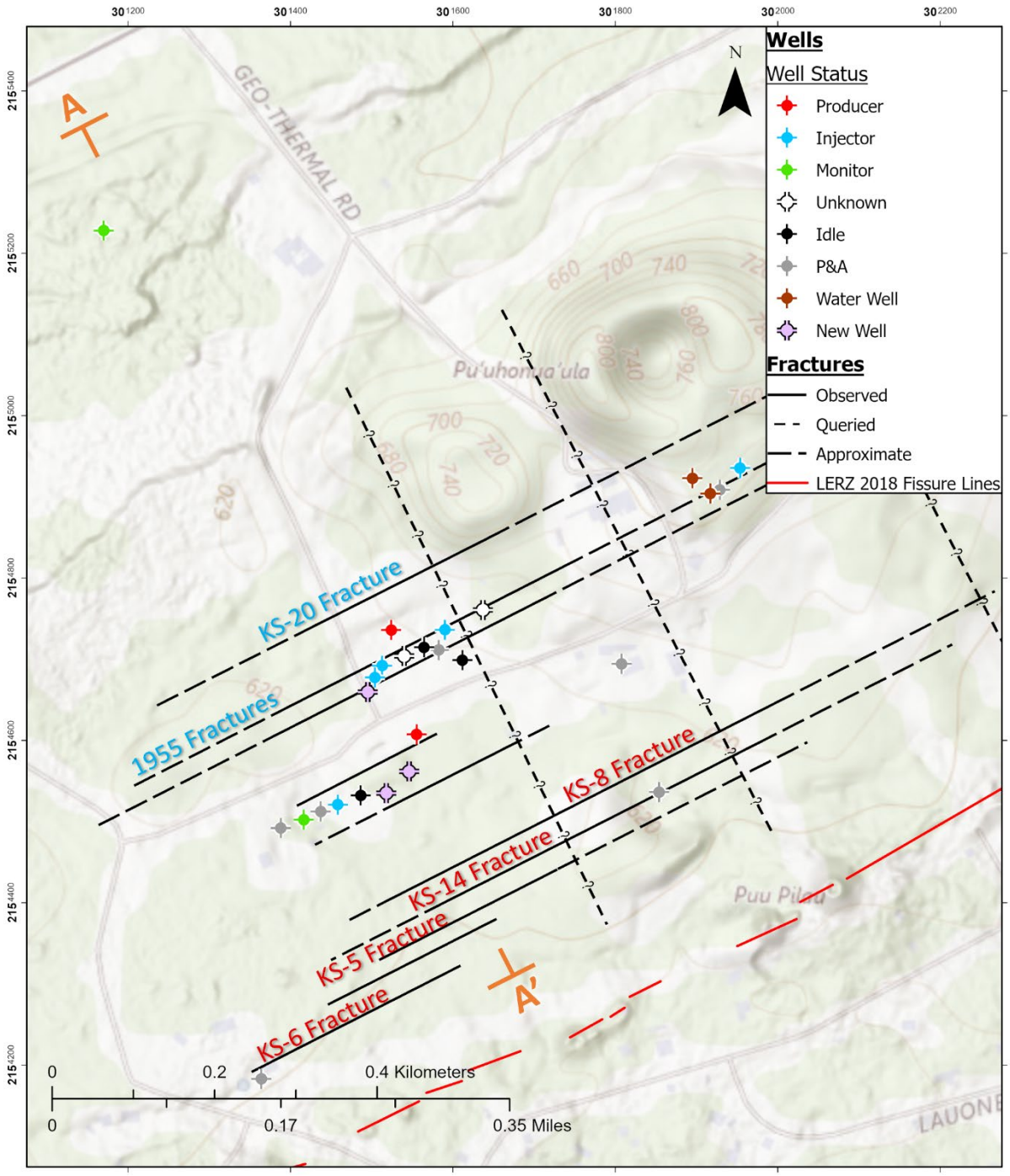

Figure 5: Map of the PGV wellfield showing known and hypothesized subsurface fracture pathways. Key production and injection structures are labeled in red and blue, respectively. Figure 10 cross section extents indicated by A-A' line (orange symbology).

2.4 Image Log Results

Borehole image logs are an invaluable dataset which allow quantification of fracture attitudes and in some cases the orientation of the stress field, data points which allow ground truthing of key elements of a conceptual model, and for this reason acquisition of an acoustic image log was an important component of the logging and testing plan for the northernmost well drilled in the 2022-2023 campaign. The borehole geometry and stability conditions were considered continuously throughout drilling and the decision-making process of calling TD, and these components were essential to making an informed, risk-based plan and decision for log acquisition. For example, below 6900 ft MD the borehole "inverts", changing azimuth by ~180° as designed to re-cross the target fracture zone, and this geometry was an important component of selecting the image log interval. With no significant fill on bottom observed during drilling or reaming (which could indicate borehole sloughing or collapse), the borehole was considered to be in stable condition and approval was granted to run a PTS survey followed by image log acquisition. However, to maintain borehole stability throughout logging operations it was decided that the wellbore would remain filled with drilling mud rather than switching over to water, as is common for acquisition of acoustic image logs.

The image log was successfully acquired from the casing shoe (3634 ft) to 6900 ft MD. The image quality is poor overall due to suspended solids in the fluid column from the drilling mud causing attenuation of the acoustic signal, but interpretation of important features is still possible. Analysis of the image log identified 248 discrete features over the 3266 ft log interval. Most structures identified are rift-parallel and sub-vertical, dipping both NNW and SSE (supporting key elements of the conceptual model), with a minor population of NW-trending, SW-dipping features identified.

Southeast-striking (rift-cutting) fractures captured in the image log have strikes ranging from ±105°-160°, with the mode of the population oriented approximately 112°/75° (strike/dip) (Figure 6). Mapped surface representations of these features, represented as queried fractures in Figure 5, strike 154°; this attitude is based on combined analysis of regional to local gravity and magnetic surveys, LiDAR lineaments, and tracer studies, and is consistent with the range of fracture attitudes implied by image log interpretation. Whether there are throughgoing, high permeability fractures present in the field, as the mapped traces imply, or if NW-SE trending fractures are found as a distributed population throughout the subsurface, as they manifest in the image log interval, is a remaining uncertainty in the conceptual model with important implications for reservoir management and well targeting.

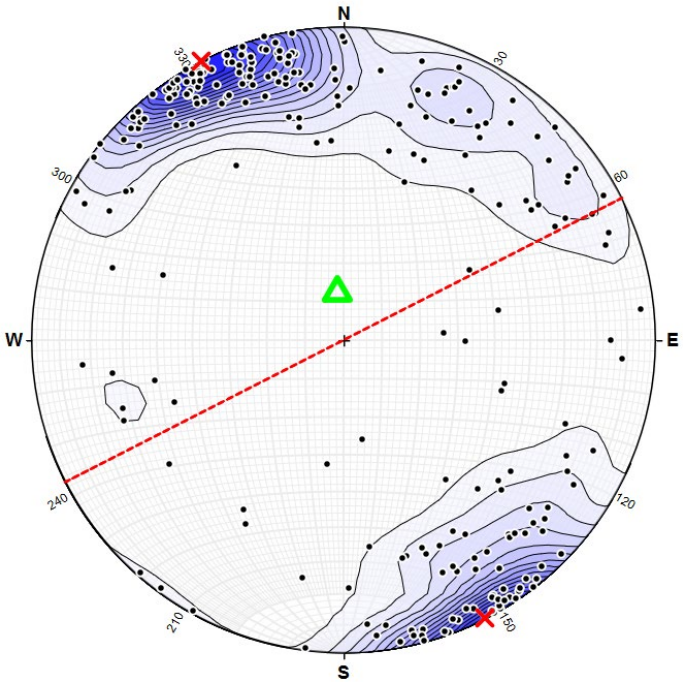

Figure 6: Lower hemisphere stereonet with poles to planes plotted and contoured for all fractures identified in the image log (n=248). The trend of the LERZ (063°/243°) is indicated by the dashed red great circle, and poles to that vertically dipping plane are indicated by red X's. The average (median) attitude of the borehole through the imaged interval is plotted as a bold green triangle.

Drilling induces damage to the borehole wall may be preserved as borehole breakouts (BO), petal-centerline fractures (PCF), or drilling induced tensile fractures (DITF), structures which can be used to infer the orientation of the modern stress state in the subsurface (e.g., Davatzes and Hickman, 2010; Moos and Zoback, 1990, Zoback et al., 1985). Three pairs of DITFs were identified in the image log. DITFs at ±3650 ft and 4450 ft are oriented NE-SW, indicating that S_{Hmax} is roughly aligned with the trend of the LERZ (Figure 7) and fractures subparallel to the rift should be well-oriented for dilation and fluid flow (e.g., Heffer, 2002). However, the final pair of DITFs identified at ±6270 ft are oriented NW-SE (116°/299°), an approximately 60° shift from the shallower pairs, which would place rift-parallel fractures under compression and preferentially favor fluid flow along NW-SE trending structures. This rotation may be local, with the attitude of S_{Hmax} reverting to a NE-SW orientation beyond the logged interval. Alternatively, this stress field rotation may imply that deep permeable zones in the northern wellfield are more likely to be channelized along rift-perpendicular fractures, which may facilitate rapid breakthrough of injectate back to the production field and thus unfavorable cooling of the reservoir. Additional testing, particularly a long-term reservoir tracer test, is required to better understand the fluid pathways from the injection to production fields.

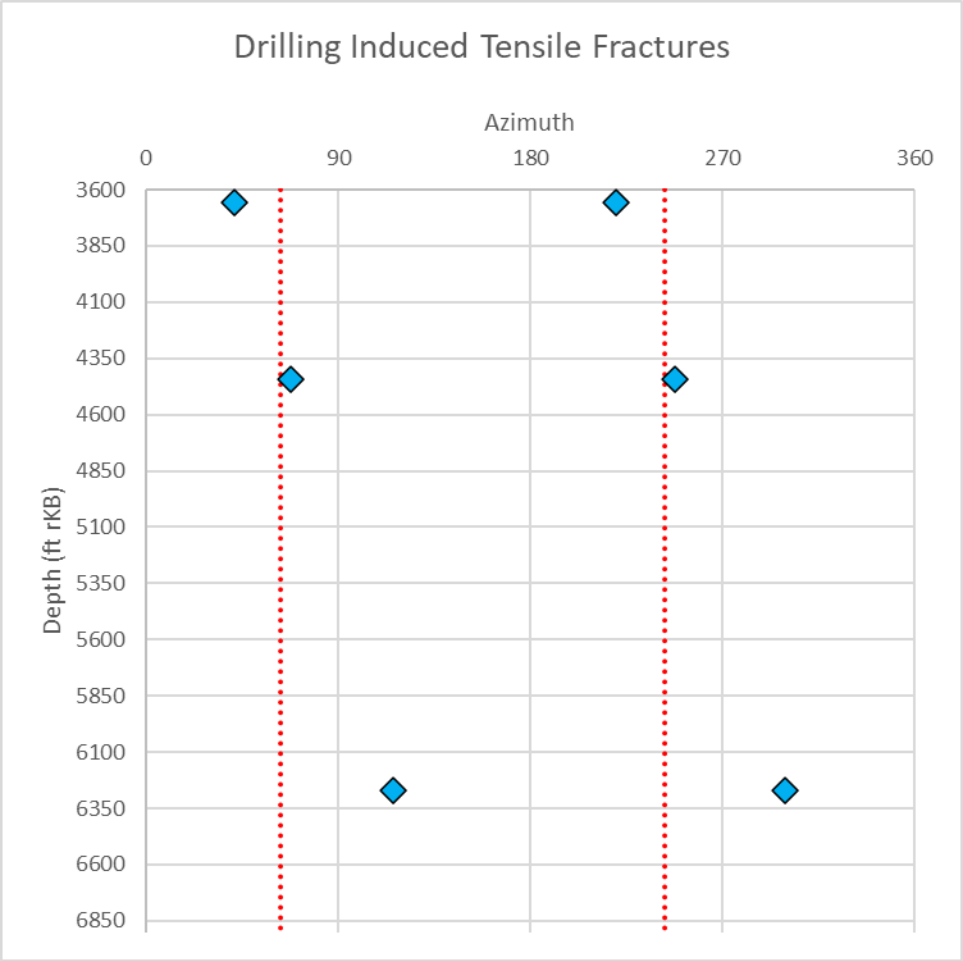

Figure 7: Drilling induced tensile fractures (blue diamonds) identified in image log plotted against borehole depth. The trend of the LERZ is plotted as red dotted lines.

2.5 Alteration Systematics

Hydrothermal alteration of basaltic to diabasic host rocks occurs as replacement mineralization and fracture or vesicle filling secondary mineral deposits. Replacement minerals include clays, chlorite, and disseminated pyrite, with replacement mineralization first appearing at ±1500 ft MD (±455 m) and becoming more pervasive below ±4000 ft MD (±1220 m).

High clay content logged in drill cuttings is a function of both temperature-dependent alteration processes and host rock lithology, with abundant clay found in glassy hyaloclastites of the transitional zone/near shore depositional environment. Widespread clay begins at ±2600 ft (792 m) bgl (-1110 ft/ -580 m rSL) and is logged to variable depths that are interpreted to represent the size and shape of the clay caprock overlying the convective hydrothermal system. Thick expanses of clay are interbedded with unaltered basalt flows and hyaloclastite deposits, indicating the incomplete alteration of the host rock and imperfect nature of the caprock. This incomplete alteration combined with structural discontinuities from tectonic fracturing allow minor leakage of fluids and steam from the underlying hydrothermal system in the natural state. This phenomenon is well-documented in geothermal systems around the world where surface manifestations

overlying the reservoir document leakage of steam and fluids through the caprock (e.g., Rowland and Simmons, 2002).

Four distinctive fracture filled mineral assemblages are recognized. The stratigraphically highest, lowest temperature assembly consists of amorphous silica (opaline silica and chalcedony) + anhydrite + pyrite ± clay/chlorite ± zeolite(s) ± calcite. A moderate to high temperature assemblage is composed of anhydrite + pyrite + quartz + chlorite ± garnet ± chalcopyrite. The highest temperature, deepest stratigraphic assemblage consists of quartz + epidote + chlorite ± actinolite ± anhydrite.

A quantitative relationship between reservoir temperatures and these mineral assemblages has not been well established due to the propensity of higher temperature fluids from deep in the reservoir to flow upwards within the wellbore and mask the flow from the upper, cooler entries. From mineralogical and fluid temperature correlations from other known geothermal fields, the low temperature mineral assembly probably represents reservoir temperatures of 300-400°F, the moderate temperature assembly represents temperatures of 400-550°F, and the high temperature group ≥550°F.

Mineralogical precursors to entry into high-temperature production zones are not well-developed in the Puna field. In shallower portions of the high-temperature system, such as that encountered in KS-7, a hydro-fractured texture consisting of brecciated basalt, re-cemented with silica and anhydrite, may be present along with bladed pyrrhotite. Below 3500 ft depth, minor occurrences of euhedral epidote have been noted within 100 feet of entry into producing fractures. However, it is stressed that mineralogical precursors may be rare or absent immediately prior to entry into a producing fracture.

3. Geophysics

Geophysical data acquired near PGV reveal that measurable variations within the rocks of the LERZ are subtle, primarily due to the island's lithologic homogeneity. Gravity data indicate a lack of significant density contrast between rock units, resulting in a relatively attenuated gravitational signature. Several generations of resistivity surveys have been completed with varying degrees of success, including 4 CSAMT lines in 1993 and a regional magnetotelluric (MT) survey focused on imaging magma reservoirs and conduits within Kilauea and the East and Southwest rift zones. While the CSAMT data is of limited use due to the high levels of anthropogenic noise near the power plant, Hoversten et al. (2022) demonstrates that MT resolves the rift zones as extensive low resistivity anomalies and provides insight into successful MT acquisition in the challenging field conditions found near Kilauea.

An airborne magnetic survey collected in 1978 with flight line spacings of 0.8 and 1.6 km demonstrated that magnetics is a useful tool for imaging the regional structure of the LERZ (Flanigan & Long, 1987). Ormat collected an airborne magnetic survey over PGV which enhances the resolution of key features, revealing strong magnetic highs that correlate with mapped eruptive vents and faults along the LERZ (Reynolds et al., 2024). The survey shows that sharp magnetic highs aligned with the trend of the LERZ, interpreted as shallow dikes with high magnetic susceptibility, make a left-step near PGV, consistent with the rift geometry implied by vents and fissures. Lineaments linking the two main rift segments in this area trend approximately perpendicular to the rift, supporting the existence of NW-SE (±333°/153°) trending fractures in

the vicinity of the geothermal system. It should be noted that the survey is not interpreted as imaging alteration and destruction of magnetic minerals associated with the upper portions of the hydrothermal system due to the depth to the resource (>3000 ft). Rather, breaks in magnetic highs associated with the rift trend are interpreted as possible structures which may extend into the subsurface and influence permeability pathways (Figure 8).

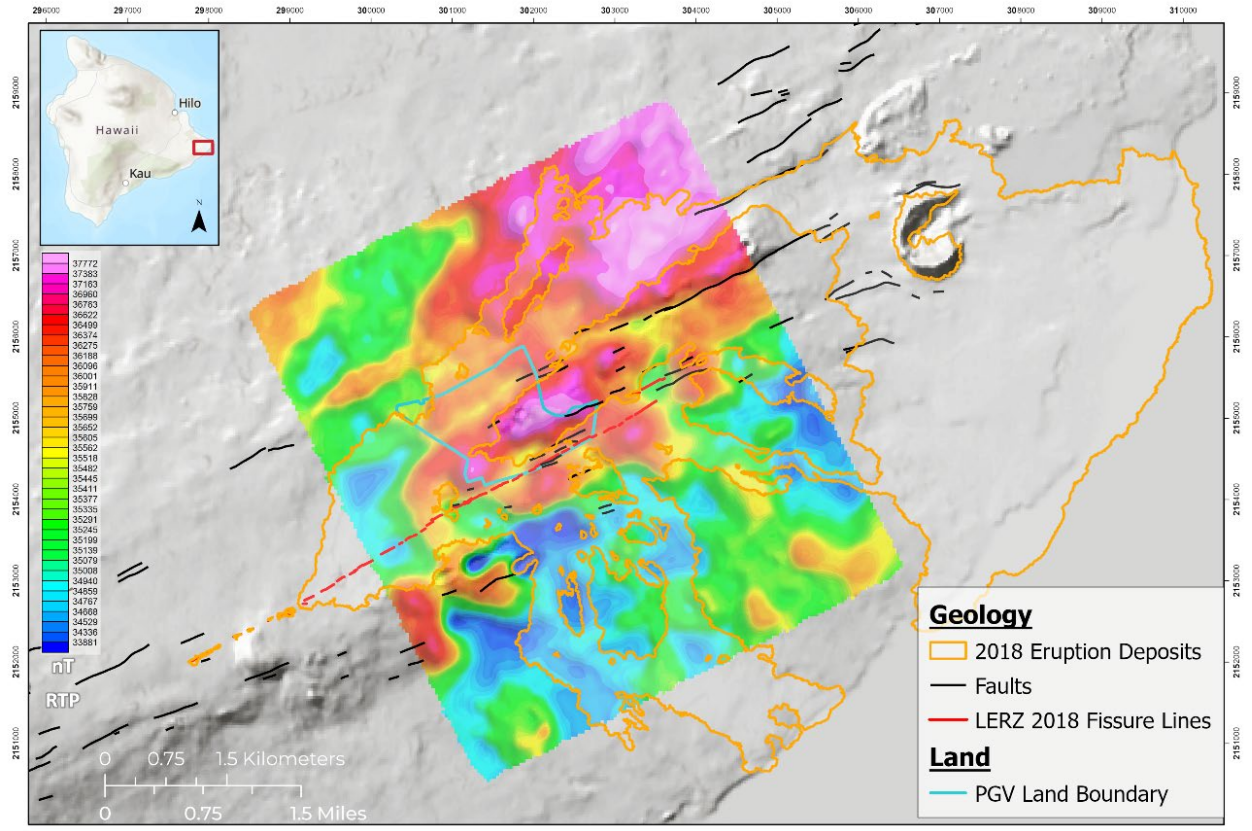

Figure 8: RTP (reduced to pole) magnetic data overlain on a 30 m DEM of the LERZ and PGV. Basalt deposits from the 2018 eruption are shown outlined in orange; mag anomalies do not follow the deposits, indicating that deeper structures are resolved by the method.

4. Geochemistry

Production fluids from PGV are a combination of two-phase flow from intra-wellbore boiling, as well as two-phase brine and steam in the reservoir based on enthalpy measurements and quarterly tracer flow tests (TFTs). Reservoir brines at PGV are moderate TDS (up to ±23,000 ppm), Na-Cl fluids with reservoir pH generally estimated between 5-6. The fluids are variably mixed, thermally altered meteoric-modified seawater brine with up to 70% modified seawater (Figure 9). Gas composition is dominated by H_2S and CO_2 with total discharge of less than 0.5 wt.%.

The basal groundwater aquifer above the PGV hydrothermal resource is predominantly a mixture of meteoric and altered seawater, with temperatures ranging between 30-65°C. The basal aquifer within the LERZ experiences a high degree of natural spatial and temporal chemical heterogeneity. This is likely a result of near well structures, such as highly permeable lava flows being intersected with impermeable dikes, which may isolate shallow aquifers and limit fluid flow. In addition to

structural controls, changes in the rates of recharge into these aquifers varies the degree of input from seawater versus meteoric water sources (Novak, 1995; Thomas, 1987 and Sorey and Colvard, 1994). Further, some minor degree of natural steam leakage into the system is inferred based on slightly depressed pH values and elevated sulfate concentrations in some monitoring wells such as MW-1.

There are no surface manifestations related to the PGV system. There are, however, a series of warm springs and seeps that occur to the SSE along the coast and isolated steam vents within the rift associated with the 1955 and 2018 fissure eruptions. Based on lower expected resource temperatures inferred from geothermometery and differences in the degree of seawater dilution, the springs are hypothesized to be related to a separate hydrothermal system (Janik et al., 1994).

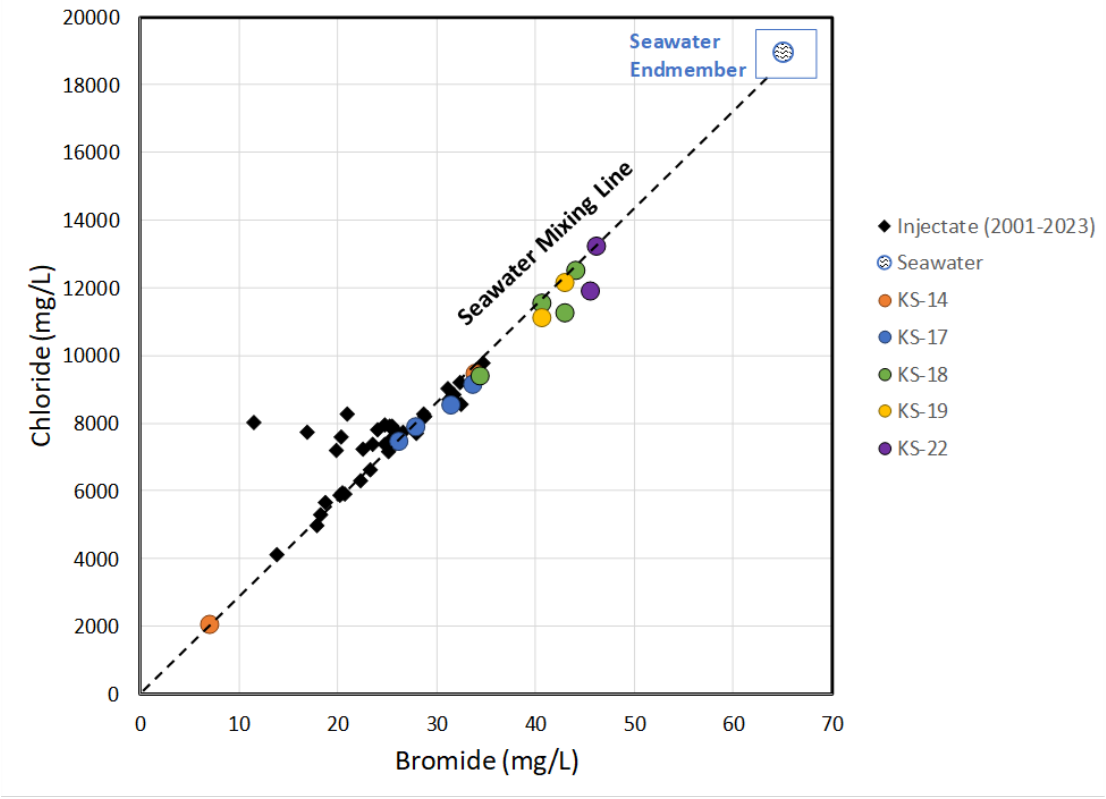

Figure 9: Chloride/Bromide cross plot showing the relationship between PGV brines and seawater. Production brines and injectate plot on the seawater mixing line.

5. Conceptual Model

The Puna reservoir is a high temperature, two-phase, liquid-dominated system with a varying steam fraction confined within Kilauea's Lower East Rift Zone. Heat for the system is supplied by active magma migration and the very high heat flow through the rift. Intrusion of magma into the rift zone displaces the southern flank of the volcano, promoting dilation along the rift. A prominent left step in the rift in the vicinity of PGV generates and maintains a zone of locally enhanced permeability in basalt flows and dikes with low natural porosity and permeability. The high permeability production and injection structures are subvertical, rift-parallel fractures that often associate with diabase dike margins, with fractures perpendicular to the rift formed as a function

of the stepover facilitating injection returns to production. The system is overlain by a caprock formed by hydrothermal alteration of pahoehoe & a'a flows, hyaloclastite, and pillow basalts which alters mafic minerals and volcanic glass to smectite-rich clay. The glassy groundmass characterizing hyaloclastite makes them particularly susceptible to clay alteration and the caprock is largely coincident with the extents of these transitional marine deposits. Departures of the clay caprock from the modeled extents of the transitional zone are interpreted based on the distribution of the natural state temperatures of the system, with the caprock closely following the 200°C isotherm due to the instability of smectite clays above that temperature (e.g., Reyes, 1990). Clay alteration is not homogenous and the caprock is likely breached in places by tectonic dilation over the lifecycle of a long-lived geothermal system, but naturally occurring leakage into overlying strata is thought to be relatively minor and transient in nature as the leaking structure self-seals due to hydrothermal alteration. Surface manifestations are suppressed by the deep resource depths, the clay caprock, and the vigorous groundwater system overlying the reservoir, all working in conjunction to keep the system hidden at surface. The water table within the resource area occurs at an elevation of approximately sea level (0 mRSL), corresponding to a depth of 188m (620 ft).

The distribution of interpreted static-state temperatures in PGV suggest that upflow originates along steeply northwest-dipping fractures. Note that the isotherms displayed in Figure 10 represent the post-eruption conditions, not the natural state of the system, and reflect significant cooling of the northern reservoir by a long history of injection.

Steep NW-SE thermal gradients through the field are a function of high permeability and convection along sub-vertical fractures within the rift zone versus unfractured zones adjacent to the rift to the north and south. The occurrence of permeable rift-perpendicular fractures as integrated into the conceptual and numerical models based on surface geology and tracer returns, a hypothesis which has been further substantiated by a recent airborne magnetic survey, which clearly images the left-step in the LERZ, and analysis of an acoustic borehole image log, which demonstrates the existence of NW-SE trending fractures throughout the logged interval. However, a key uncertainty remaining in the conceptual model is whether (a) there are large, high permeability NW-SE pathways (as the queried faults in Figure 5 would imply), or (b) NW-SE trending fractures represent a distributed fracture set that is present throughout the field but not localized into a handful of high permeability pathways.

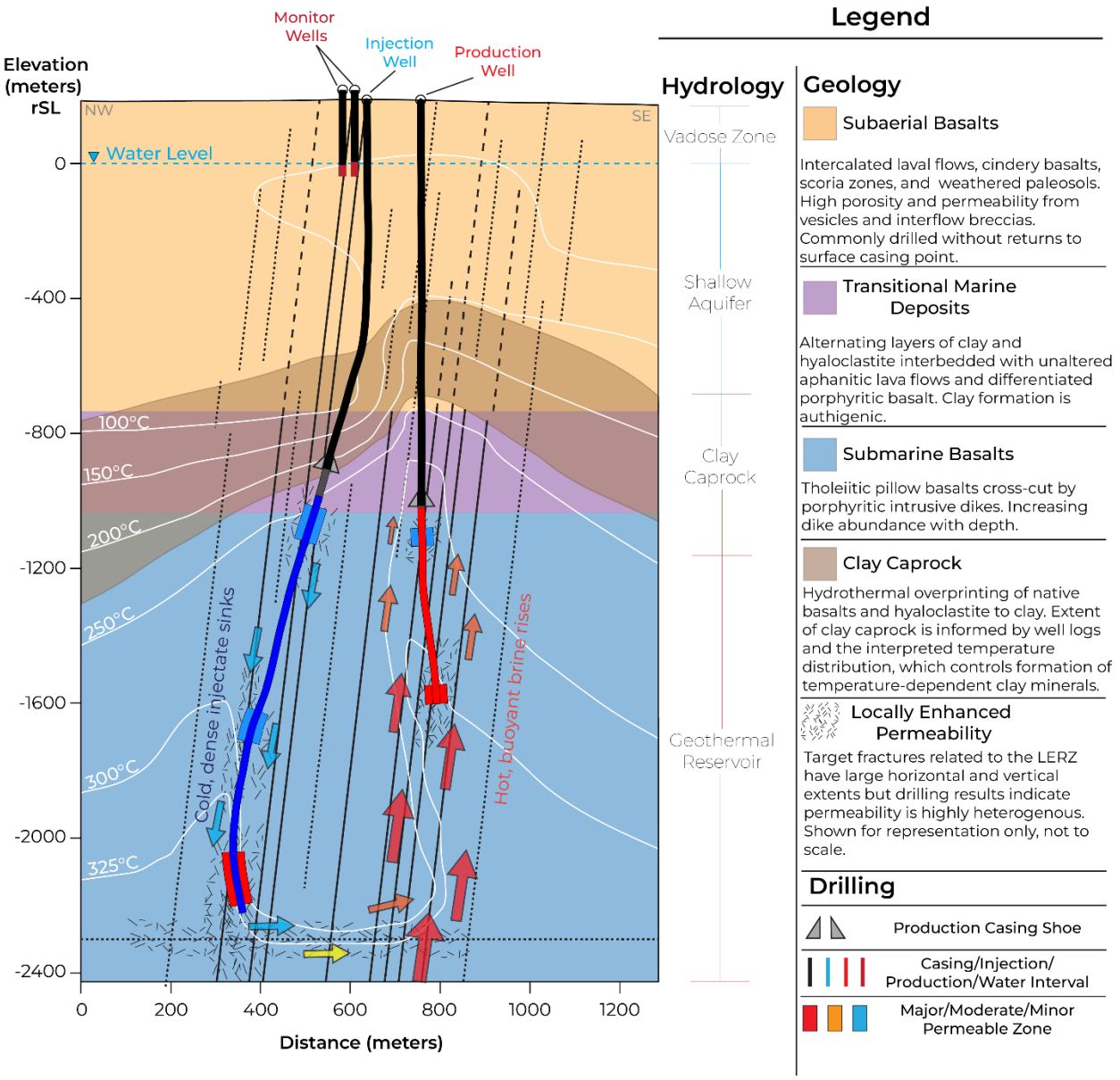

Figure 10: Schematic diagram of the PGV hydrothermal system conceptual model, including interpreted post-eruption natural state isotherms which depict significant cooling of the reservoir at injection depths. Vertical exaggeration 0.75x.

6. Conclusion

The Puna Geothermal Venture represents a high-temperature, naturally occurring geothermal system found in the active Lower East Rift Zone of Kilauea. The geothermal system's location is due in part to the occurrence of a prominent left-step in the rift zone which creates locally enhanced permeability. Fracture-dominated permeability and upflow of thermal fluids at PGV are controlled primarily by rift-parallel fractures. Rift-perpendicular permeability pathways were previously hypothesized based on surface mapping, geophysical datasets, and reservoir tracer studies, and have been confirmed for the first time at PGV by analysis of an acoustic borehole image log. Additional reservoir testing is required to understand the impact of rift-perpendicular fractures and

the connection between production and injection following the successful completion of a recent drilling campaign.

7. Acknowledgements

We would like to thank the PGV operators, Ormat's Wellfield and Resource staff who contributed to post-eruption recovery effort and who continue to operate and maintain PGV as a flagship geothermal power plant, as well as Peter Drakos for his more than 15 years of geoscience contribution to the field.

REFERENCES

Broyles, M. L., Suyenaga, W., & Furumoto, A. S., "Structure of the lower east rift zone of Kilauea volcano, Hawaii, from seismic and gravity data," Journal of Volcanology and Geothermal Research, 5(3-4), (1979), 317-336.

Clague, D. A., & Dalrymple, G. B., "The Hawaiian-emperor volcanic chain," US Geol. Surv. Prof. Pap., 1350, (1987), 5-54.

Davatzes, N. C., & Hickman, S. H., "The feedback between stress, faulting, and fluid flow: Lessons from the Coso Geothermal Field, CA, USA," in Proceedings World Geothermal Congress, Vol. 2010, (April 2010).

Department of Planning and Economic Development (DPED), State of Hawaii, "Geothermal Power Development in Hawaii. Volume I. Review and Analysis," Department of Energy Report, DOE/ET/27133, (1982).

Duffield, W.A., "Structure and origin of the Koae fault system, Kilauea Volcano, Hawaii." USGS Professional Paper 856. (1975).

Eaton, J. P., & Murata, K. J., "How Volcanoes Grow: Geology, geochemistry, and geophysics disclose the constitution and eruption mechanism of Hawaiian volcanoes," Science, 132(3432), (1960), 925-938.

Flanigan, V.J., & Long, C.L., "Aeromagnetic and Near-Surface Electrical Expressions of the Kilauea and Moana Loa Volcanic Rift Systems," Volcanism in Hawaii, 1, pg. 935-946, (1987).

Furumoto, A. S., MacDonald, G. A., Druecker, M., & Fan, P. F., "Preliminary studies for geothermal exploration in Hawaii, 1973-1975," (1977).

Heffer, K., "Geomechanical influences in water injection projects: An overview," Oil & Gas Science and Technology, 57(5), (2002), 415-422.

Hoversten, G.M., Gasperikova, E., Mackie, R., Myer, D., Kauahikaua, J., Newman, G.A., Cuevas, N., "Magnetotelluric Investigations of the Kilauea Volcano, Hawaii," Journal of Geophysical Research: Solid Earth, 127.8, (2022).

Janik, C.J., Nathenson, M., & Scholl, M.A. "Chemistry of spring and well waters on Kilauea Volcano, Hawaii, and vicinity." USGS Open File Report 94-586, (1994).

Kinoshita, W.T., Krivoy, H.L., Mabye, D.R., MacDonakd, R.R., "Gravity survey of the island of Hawi'i, Geologic Survey Research 1963," U.S. Geol. Surv. Prof. Pap., 475, (1963), 114-116.

Langenheim, V. A., & Clague, D. A., "The Hawaiian-Emperor Volcanic Chain. Part II. Stratigraphic framework of volcanic rocks of the Hawaiian Islands," USGS Prof. Pap, 1350, (1987), 55-84.

Lautze, N., Thomas, D., Hinz, N., Apuzen-Ito, G., Frazer, N., & Waller, D., "Play fairway analysis of geothermal resources across the State of Hawaii: 1. Geological, geophysical, and geochemical datasets," Geothermics, 70, (2017), 376-392.

Lipman, P. W., Lockwood, J. P., Okamura, R. T., Swanson, D. A., & Yamashita, K. M., "Ground deformation associated with the 1975 magnitude-7.2 earthquake and resulting changes in activity of Kilauea volcano, Hawaii," (1985), No. 1276.

Lipman, P. W., Sisson, T. W., Ui, T., Naka, J., & Smith, J. R., "Ancestral submarine growth of Kilauea volcano and instability of its south flank," in Hawaiian volcanoes: deep underwater perspectives, 128, (2002), 161-191.

Moore, R. B., "Volcanic geology and eruption frequency, lower east rift zone of Kilauea volcano, Hawaii," Bulletin of Volcanology, 54, (1992), 475-483.

Moore, R. B., & Trusdell, F. A., "Geologic map of the lower east rift zone of Kilauea Volcano, Hawaii," (1991), No. 2225.

Morgan, W. J., "Convection plumes in the lower mantle," Nature, 230(5288), (1971), 42-43.

Moos, D., & Zoback, M. D., "Utilization of observations of well bore failure to constrain the orientation and magnitude of crustal stresses: application to continental, Deep Sea Drilling Project, and Ocean Drilling Program boreholes," Journal of Geophysical Research: Solid Earth, 95(B6), (1990), 9305-9325.

Murphy, J., Prina, N., Spielman, P., & Spake, D., "Permeability and Numerical Modeling of the Puna Geothermal Venture," GRC Transactions, Vol. 48, (2024).

Patrick, M. R., Houghton, B. F., Anderson, K. R., Poland, M. P., Montgomery-Brown, E., Johanson, I., ... & Elias, T., "The cascading origin of the 2018 Kīlauea eruption and implications for future forecasting," Nature Communications, 11(1), (2020), 5646.

Poland, M. P., Miklius, A., & Montgomery-Brown, E. K., "Magma supply, storage, and transport at shield-stage Hawaiian volcanoes," (2014), No. 1801-5, 179-234.

Novak, S.P. "A conceptual model of shallow groundwater flow within the Lower East Rift Zone of Kilauea Volcano, Hawaii." Masters Thesis, University of Hawai'i at Manoa. Honolulu, Hawaii, 170, (1995).

Rowland, J.V., & Simmons, S.F., "Hydrologic, magmatic, and tectonic controls on hydrothermal flow, Taupo Volcanic Zone, New Zealand: Implications for the formation of epithermal vein deposits." Economic Geology 107, no.3, 427-457, (2012)

Reyes, A. G., "Petrology of Philippine geothermal systems and the application of alteration mineralogy to their assessment," Journal of Volcanology and Geothermal Research, 43(1-4), (1990), 279-309.

Reynolds, Z., Spake, D., Caro, D., Prina, N., Feucht, D., Blake, K., Libbey, R., & Delwiche, B., “Detailed Airborne Magnetic Survey of the Puna Geothermal Venture and the Lower East Rift Zone, Island of Hawai’i,” GRC Transactions, Vol. 48 (2024).

Ryan, M. P., "The mechanics and three-dimensional internal structure of active magmatic systems: Kilauea Volcano, Hawaii," Journal of Geophysical Research: Solid Earth, 93(B5), (1988), 4213-4248.

Sherrod, D. R., Sinton, J. M., Watkins, S. E., & Brunt, K. M., "Geologic map of the State of Hawaii," (2021), No. 3143.

Sorey,M.L., & Colvard, E.M., “Potential Effects of the Hawaii Geothermal Project on Ground-Water Resources on the Island of Hawaii.” Water Resources Investigation Report 94-4028, USGS, (1994).

Swanson, D. A., Duffield, W.A., & Fiske, R.S., "Displacement of the south flank of Kilauea volcano: The result of forceful intrusion of magma into the rift zones," US Geol. Surv. Prof. Pap., 963, (1976), 39.

Takahashi, P., Seki, A., & Chen, B., "A Pacific-wide geothermal research laboratory: the Puna Geothermal Research Facility," Uniiversity of Hawaii, 2540 Dole Street, Honolulu, Hawaii 96822, (1985), No. SGP-TR-84; CONF-850107-33.

Thomas, D. M., "Geothermal resources assessment in Hawaii," Geothermics, 15(4), (1986), 435-514.

Thomas, D.M., , “Geochemical model of the Kilauea east rift zone.” Volcanism in Hawaii, ch. 56. (1987) U.S. Geological Survey Open File Report 93-82.

Trusdell, F.A., Novak, E., Evans, S.R., & Okano, K., "Core lithology from the State of Hawaii Scientific Observation Hole 1, Kilauea Volcano, Hawaii," U.S. Geological Survey Open-File Report 99–389, (1999), 67 p., http://hdl.handle.net/10125/21548.

Warren, I., Friedel, M. J., Wallin, E., Lautze, N., Hou, Z. J., Vasco, D. W., ... & Rhodes, G., "Innovative Subsurface Learning and Hawaiian Exploration using Advanced Tomography (ISLAND HEAT) Phase 1 Final Report," National Renewable Energy Laboratory (NREL), Golden, CO (United States), (2023), No. NREL/TP-5700-87316.

Wilson, J. T., "A possible origin of the Hawaiian Islands," Canadian Journal of Physics, 41(6), (1963), 863-870.

Zoback, M. D., Moos, D., Mastin, L., & Anderson, R. N., "Well bore breakouts and in situ stress," Journal of Geophysical Research: Solid Earth, 90(B7), (1985), 5523-5530.

Zoeller, M. H., Perroy, R. L., Wessels, R., Fisher, G. B., Robinson, J. E., Bard, J. A., Peters, J., Mosbrucker, A., & Parcheta, C. E., "Geospatial database of the 2018 lower East Rift Zone eruption of Kilauea Volcano, Hawaii [Data set]," U.S. Geological Survey, https://doi.org/10.5066/P9S7UQKQ.